Water Research, Volume 205, October 2021, Article number 117657
DOI:10.1016/j.watres.2021.117657

Reducing arsenic toxicity using the interfacial oxygen nanobubble technology for sediment remediation

Ying Tang[a,b], Meiyi Zhang[b], Jing Zhang[b], Tao Lyu[c], Mick Cooper[d], Gang Pan[b,d*]

[a] *Chongqing Key Laboratory of Soil Multi-Scale Interfacial Process, Department of Soil Science, College of Resources and Environment, Southwest University, Chongqing 400715, P. R. China*

[b] *Research Center for Eco-Environmental Sciences, Chinese Academy of Sciences, Beijing 100085, P. R. China*

[c] *Cranfield Water Science Institute, Cranfield University, College Road, Cranfield, Bedfordshire, MK43 0AL, UK*

[d] *Integrated Water-Energy-Food Facility (iWEF), School of Animal, Rural, and Environmental Sciences, Nottingham Trent University, Nottinghamshire NG25 0QF, UK*

[*] ***Corresponding authors: gang.pan@ntu.ac.uk (Gang Pan)***

Abstract

The arsenic (As)-bearing eutrophic waters may suffer from the dual conditions of harmful algal blooms and release of As, driven by algal-induced hypoxia/anoxia. Here, we investigate the use of interfacial oxygen (O_2) nanobubble technology to combat the hypoxia and control As exposure in simulated mesocosm experiments. It was observed that remediation of algal-induced hypoxia at the sediment-water interfaces (SWI) by application of O_2 nanobubbles reduced the level of dissolved As from 23.2 μg L^{-1} to <10 μg L^{-1} and stimulated the conversion of As(III) to the less toxic As(V) (65–75%) and methylated As (10–15%) species. More than half of the oxidation and all the methylation of As(III) resulted from the manipulation by O_2 nanobubbles of microbes responsible for As(III) oxidation and methylation. Hydroxyl radicals were generated during the oxidation of reductive substances at the SWI in darkness, and should be dominant contributors to

Published by Elsevier. This is the Author Accepted Manuscript issued with: Creative Commons Attribution Non-Commercial No Derivatives License (CC:BY:NC:ND 4.0).
The final published version (version of record) is available online at DOI:10.1016/j.watres.2021.117657. Please refer to any applicable publisher terms of use.

As(III) abiotic oxidation. X-ray absorption near-edge structure (XANES) spectroscopic analysis demonstrated that surface sediments changed from being sources to acting as sinks of As, due to the formation of Fe-(hydr)oxide. Overall, this study suggests that interfacial O_2 nanobubble technology could be a potential method for remediation of sediment As pollution through the manipulation of O_2-related microbial and geochemical reactions.

Keywords: Eutrophic waters; Arsenic oxidation; Nanobubble; Hypoxia remediation; Arsenic metabolism functional genes; Hydroxyl radicals

1. Introduction

Levels of Arsenic (As) are increasing in the environment and posing threats in surface water ecosystems (e.g. rivers and lakes) through both natural and anthropogenic activities (Weber et al., 2010; Zhang et al., 2018a). Drinking water directly derived from such contaminated sources poses a human health risk for more than 150 million people globally (Kay, 2011). Moreover, bioaccumulation and magnification of As through aquatic foods web, and uptake it by crops through irrigation with As-contaminated water also significantly contribute to public health issues (Huang, 2016).

In aquatic environments where the bottom water–is well-oxygenated, As is commonly bound with Fe, Mn, and organic carbon within the sediment (Couture et al., 2010). Harmful algal blooms (HABs) are increasing in aquatic ecosystems globally, owing to increases in episodic eutrophication and as a consequence of global warming (Huisman et al., 2018; Pan et al., 2018). The subsequent oxygen (O_2) depletion by

mineralization of senescent algal blooms induces hypoxia/anoxia at the sediment-water interfaces (SWI) (Lei et al., 2019; Tang et al., 2019). Previous field investigations have demonstrated that eutrophication induced hypoxia/anoxia might favour the reductive dissolution of As(V)/As(III)-bearing iron oxides in the surface sediments, and thus induce ~~its~~ endogenous release of As to the water column (Hasegawa et al., 2009; Yan et al., 2016). Moreover, reduction of As(V) to As(III) (a more toxic As species) could be stimulated by the activity of indigenous As(V)-reducing~~tive~~ microbes under hypoxic/anoxic conditions (Tang et al., 2019). Therefore, combating the hypoxic/anoxic conditions at the SWI could be an efficient strategy by which to control As levels and toxicity in eutrophic surface waters.

Traditional oxygenation methods, such as deep water aeration and the artificial mixing of surface and bottom waters (Bierlein et al., 2017), have been reported to be effective to some extent. However, these approaches have been hindered when used in large and/or deep waters, due to their capital costs and energy consumption (Bormans et al., 2016; Funkey et al., 2014). The capital cost of installation of pumps in a deep water body is estimated to cost approximately €0.3 million/km^2 (Stigebrandt and Gustafsson, 2007; Zhang et al., 2021). Additional operational costs of nearly €0.2-0.25 million/km^2/year may be incurred, due to the continuous operation required during the summer season, or even the whole year, in order to maintain the O_2 supply and resultant nutrients/pollutants control at the SWI (Bormans et al., 2015; Johnston et al., 2011). Moreover, the induced massive hydraulic disturbance caused by traditional aeration methods through pumps may trigger the re-suspension of anoxic sediments. Such re-suspended sediments could release the long-term buried pollutants/nutrients back to the

water column and increase the O_2 consumption (Bormans et al., 2015). Furthermore, the change of the status could affect the stable habitats for the benthic biota (Zhang et al., 2021).

In order to overcome these drawbacks, the interfacial O_2 nanobubble technology has been developed and attempted to address this issue in a cost-effective and environmental-friendly way (Zhang et al., 2018b). This approach utilises natural minerals loaded with O_2, which could deliver nanoscale O_2 bubbles (bubble size < 1 μm) after settling into the sediment surface by natural gravity. The earlier study also demonstrated synergy between the diffusion of O_2 nanobubbles and retention of O_2 in the surficial sediment layer, which successfully reversed the hypoxic conditions and maintained high levels of dissolved O_2 (6 mg L^{-1}) at the SWI over a period of 4 months (Zhang et al., 2018b). The successful performance could be attributed mainly to the novel physical and chemical features of nanobubbles including long lifespan, high gas transfer efficiency, and the capability to generate free radicals, as compared to larger bubbles (Atkinson et al., 2019; Lyu et al., 2019). However, the effects of interfacial nanobubble technology on the control, and biogeochemical cycling, of toxic metal pollutants, such as As, during sediment remediation have not, hitherto, been well understood.

Once the O_2 nanobubbles were delivered to the hypoxic/anoxic SWI through minerals acting as carriers, we expected that the resultant hypoxic/anoxic-oxic transition could trigger As(III) oxidation through both biotic and abiotic processes. On the one hand, the supply of substantially dissolved O_2 may have stimulated the growth of the indigenous As(III) oxidizing microbes and induced biotic oxidation of As(III) to less toxic As(V) (Maguffin et al., 2015), which is prone to be immobilized by iron oxides minerals (Luong

et al., 2018). On the other hand, the abiotic process of As(III) oxidation may have been caused by the generated hydroxyl radicals (•OH), as a highly reactive and unselective oxidant, during the nanobubble treatment. Previous studies have proved that •OH could be generated along with the natural bursting of O_2 nanobubbles (Atkinson et al., 2019). Moreover, the oxygenation of anoxic sediment/water containing abundant ferrous minerals and reduced organic matter may also produce abundant •OH through Fenton or Fenton-like processes in darkness (Liao et al., 2019a; Liao et al., 2019b; Tong et al., 2016). The accompanied variation in concentration and speciation of Fe and organic matter may influence their bioavailability to microbial activity (Tang et al., 2019; Zhu et al., 2017), and thereby indirectly affect the biotic oxidation of As(III). Thus far, the hypothesised biotic and abiotic mechanisms and their quantitative contributions on As speciation in eutrophic waters have not been investigated.

The goal of this study was to evaluate the effectiveness, and to reveal the mechanism for the mitigation of As pollution by interfacial O_2 nanobubble technology in a simulated eutrophic sediment-water system. The overlying water quality and As speciation were recorded in order to evaluate the performance of hypoxic/anoxic reversion and As immobilization at the SWI. As and Fe K-edge X-ray absorption near-edge structure (XANES) spectral analyses were used to investigate sequestration mechanisms of As in the sediment, and genes responsible for As metabolism (Tang et al., 2019) (i.e., As(III) oxidation (*aio*A), As(V) respiratory reduction (*arr*A), As(V) reduction (*ars*C), and As(III) methylation (*ars*M)) extracted from the SWI were quantified to aid in the understanding of the biotic processes of As transformation. Additionally, •OH generation and its effect on As oxidation were studied in order to evaluate abiotic effects

on As speciation.

2. Materials and methods

2.1 Sample collection and construction of mesocosm columns

Lake water and sediments were collected from Lake Dianchi (Fig. S1), which is the sixth largest freshwater lake in China and, historically, has suffered from severe As contamination and the annual occurrence of cyanobacterial blooms (Zhou et al. 2016). Concentrations of As in the sediment and water column have been recorded to reach 154 mg kg^{-1} and 7.23 μg L^{-1}, respectively (Tang et al., 2019). After transferring to the laboratory, the original lake water collected from Dianchi was filtrated through a 0.2 μm membrane (Sartorius AG, Germany), in order to minimize the background concentration of algal biomass prior to any treatment. Then the filtrated lake water (600 mL) and sediments (220 mL) were then placed in 24 plexiglass cylinders (∅64 mm, length 300 mm) in order to simulate water-sediment systems (Fig. S1). All of the mesocosm columns were stabilized under dark conditions for three weeks, then algal bloom scum (*Microcystis aeruginosa,* 250 mg dry weight L^{-1} water), collected from Lake Dianchi, was added to all columns and flocculated by starch-modified soil (Jin et al., 2019) and then allowed to settle under gravity to the sediment surface, in order to simulate algal-induced hypoxia/anoxia at the SWI.

2.2 Interfacial nanobubble materials preparation and operation

Both O_2 and N_2 nanobubble-modified zeolites were prepared by a previously-described method (Zhang et al., 2018b), the details of which are also included in the

Supporting Information. After preparation of the algae biomass and of the zeolite materials, six groups of columns (four replicates of each) were prepared as (Table S1): i) the control group; ii) the pristine zeolite (Air-Ze) treatment group; iii) the N_2 nanobubble-modified zeolite (N_2-Ze) treatment group; iv) the O_2 nanobubble-modified zeolite (O_2-Ze) treatment group; v) the sterilized control (S-control) group; and vi) the sterilized O_2 nanobubble-modified zeolite (S-O_2-Ze) treatment group. Among these mesocosms, the Air-Ze and N_2-Ze groups were designed to identify As transformations resulting solely from the physical capping treatment or from any synergistic effects accompanying nanobubble treatment, during the experimental period of 18 days at 25 °C under dark conditions. The S-control and S-O_2-Ze groups were sterilized prior to commencement of the experiment groups, to avoid any microbial contribution to the As transformation process to the greatest extent, as well as to aid in the identification of any abiotic effects. In these latter two groups, all materials, including sediments, water, zeolites and algae biomass were sterilized as described in our previous study (Tang et al., 2019). The experiment conditions for the different groups are summarized in Table S1 in the Supporting Information.

2.3 Sampling and measurement

In order to monitor water quality and As mobilization during the interfacial O_2 nanobubble treatment, DO (dissolved oxygen) and Eh (redox potential) at the SWI were measured at days 0, 2, 4, 7, 12 and 18. At the same time, the overlying water at 4 cm above the SWI was sampled from the columns in groups i-iv and filtered through a 0.45 μm membrane (Whatman, UK), to measure the total dissolved As and the As speciation,

including As(III), As(V), and methylated As (i.e. monomethylarsonate (MMA(V)) and dimethylarsinate (DMA(V))).

Due to the clearly superior performance of O_2-Ze for As mitigation, the control (i) and O_2-Ze (iv) groups were employed for further mechanistic investigations. Sediment porewater samples were collected by Rhizons MOM samplers (Rhizosphere Research Products B.V., Wageningen, The Netherlands) from 1 cm above the SWI to 4 cm below with 1-cm intervals, at days 0, 2, 4, 7, 12, and 18. As this lab-scale study was conducted in isolated, well-controlled columns, the effects of dissolved forms of Fe and organic matter as suspended particles and/or in the colloidal size range, during water sample analysis, can be neglected (Wu et al., 2001). Sediment porewater samples and the aforementioned overlying water samples were filtered through a 0.45 μm membrane prior to determination of dissolved organic carbon (DOC), dissolved Fe(II) and total dissolved Fe. At the conclusion of the experiment, the mixed sediments from depths of 0-2 cm (surface), 2-4 cm (middle) and below 4 cm (deep) were sampled in an anaerobic glove chamber. These sediment samples were used for determining total organic carbon (TOC), total Fe(II), total Fe (TFe), As(III) and total As (TAs) concentrations. From these data, the concentrations of Fe(III) and As(V) can be calculated by difference between total Fe(II) and TFe, and between As(III) and TAs, respectively. Additionally, surficial sediments from these two groups were analysed by Synchrotron Radiation microscopic X-ray Fluorescence (SR-μXRF) in order to obtain the distributions of As and Fe, and by XANES in order to quantify the major speciation of As and Fe bound in sediments under various redox conditions. The abundances of genes associated with As metabolism in the overlying water column, surficial and mid-depth sediments were also analysed for these

two groups, in order to ascertain the biotic mechanisms of As speciation. Moreover, to further identify the different contributions of biotic and abiotic processes to As oxidation, overlying water and surface sediment samples from both sterilised groups (v and vi) were also taken under the same aforementioned regime and measured for total As and As(V). These levels were then compared with those from the corresponding unsterilized groups. All details about methods of measurement may be found in the Supporting Information.

2.4 Hydroxyl radical determination

As support for the estimation of the effect of •OH on abiotic As oxidation, two batch experiments were further conducted in order to discriminate whether the •OH could be generated directly from bursting nanobubbles or by simple hypoxic sediment/water oxygenation. Because lake water usually contains other chemical species, such as reduced Fe and organic matter, which create the potential to generate •OH when exposed to O_2 (Liao et al., 2019a; Liao et al., 2019b; Tong et al., 2016), ultrapure water was used to identify the •OH forming capacity of bursting nanobubbles directly sourced from O_2-Ze materials. Specifically, samples of the prepared O_2-Ze materials (10 g) were placed into degassed ultrapure water (50 mL) in a sealed amber flask. A sample of the water was then immediately removed and again at 5 minutes (mins), 0.5 hour, 24 hours and 7 days, for measurement by electron spin resonance (ESR), of •OH production (Tong et al., 2016), details are shown in the Supporting Information. Moreover, given that O_2-Ze can support abundant dissolved O_2 for oxygenation at the SWI, oxygenation of sterilized sediment slurry was additionally conducted in order to qualitatively verify the production of •OH and its potential for As oxidation. The experimental setup was similar to that employed

by Tong et al. (2016), with some modification. Briefly, sterilised sediment (30 g) and sterilised lake water (150 mL) were mixed and stored in an anaerobic chamber filled with nitrogen (99.999%), before stirring magnetically in an open amber flask for oxygenation with dissolved O_2 from the air under dark conditions. Three treatment groups with three replicates for each were performed: (I) A blank group, carried out without oxygenation; (II) An O_2 group, conducted under continuous magnetic stirring of the slurry for oxygenation; (III) An O_2-ethanol group, to which was added ethanol (100 mmol L^{-1}) for •OH inhibition (Tong et al., 2016) accompanying the oxygenation. Slurry samples from groups I and II were taken at 5 mins and 30 mins and filtered through a 0.45 μm membrane prior to •OH determination by ESR (Tong et al., 2016), details are shown in the Supporting Information. In addition, at 0, 3, 7, 17, 24, and 48 hours after the oxygenation, slurry waters (filtered through a 0.45 μm membrane) from all groups were taken for the determination of As(V) and total As, as previously detailed.

2.5 Calculation

The total dissolved As concentrations during the 18-day experimental period were used to calculate total dissolved As fluxes across the SWI. The average flux of total dissolved As was evaluated according to the mass balance equation (Tang et al., 2019), and the accumulated total dissolved As flux over the 18-day experimental period was calculated using MATLAB 9.4 software (MathWorks, Inc, USA) by the trapezoidal method (Shi et al., 2018), based on the average flux data.

3. Results and discussion

3.1 Hypoxia and As mitigation

At the early stage, some labile, simple and low molecular weight carbon compounds, such as alcohols, ketones, sugars or amino acids, in the settled algal biomass and surface sediments are easily been biodegraded (Catalán et al., 2017; Guillemette et al., 2013), leading to rapid O_2 consumption and a consequent swift decrease of the DO to 0.1 mg L^{-1} and Eh to -140 mV at day 2 (Fig. 1A and 1B). This hypoxic condition was maintained during the entire experimental period in the control system, which indicated the potential high risk to the aquatic ecosystem if this situation had occurred in natural waters (Pan et al., 2019). Sediment capping treatments, with pristine and modified zeolites, have previously been used for control of internal phosphorus loading through the blocking of buried anaerobic substances (e.g. reduced iron, sulfide and organic matter) (Li et al., 2017). However, the physical barrier thus formed at the SWI exhibited limited effect on the remediation of hypoxia, which was indicated by the low levels of DO (<0.5 mg L^{-1}) and Eh (<-50 mV) observed in the Air-Ze and N_2-Ze groups throughout the duration of the experiment (Fig. 1). When O_2-Ze was applied and allowed to naturally settle to the sediment surface, it was observed to partly mix with the soft algal bloom scum and sediments at the SWI (O_2-Ze group). The effects of sediment capping and the sustainable O_2 nanobubble release from the O_2-Ze matrix gradually compensated for the O_2 consumption at the SWI, resulting in the increase of DO to 3.2 mg L^{-1} and Eh to 150 mV beginning from day 7. This clear reversal of hypoxia, consistent with the previous studies (Shi et al., 2018; Yu et al., 2019; Zhang et al., 2021), was directly visualized by formation of a light brown-coloured oxic layer (~1 cm thickness) at the SWI after seven days (Fig. 1 and S2). The observation of such oxic layer was well aligned with the previous findings (Zhang et al., 2018b), up to 4-cm depth of sediments turned to light brown color after the

treatment by O_2-Ze for 127 days. This oxic layer was formed by the downward penetration of O_2, from O_2 nanobubbles~~,~~ into surficial sediments. It could, furthermore, provide an element of physical isolation, preventing the upwards diffusion of reduced substances from the anoxic layer into the water column and subsequent consumption of O_2~~,~~. Therefore, the generated oxic layer was contributed ~~contributing~~ to an oxic condition persistent for weeks or even months (Zhang et al., 2018b).

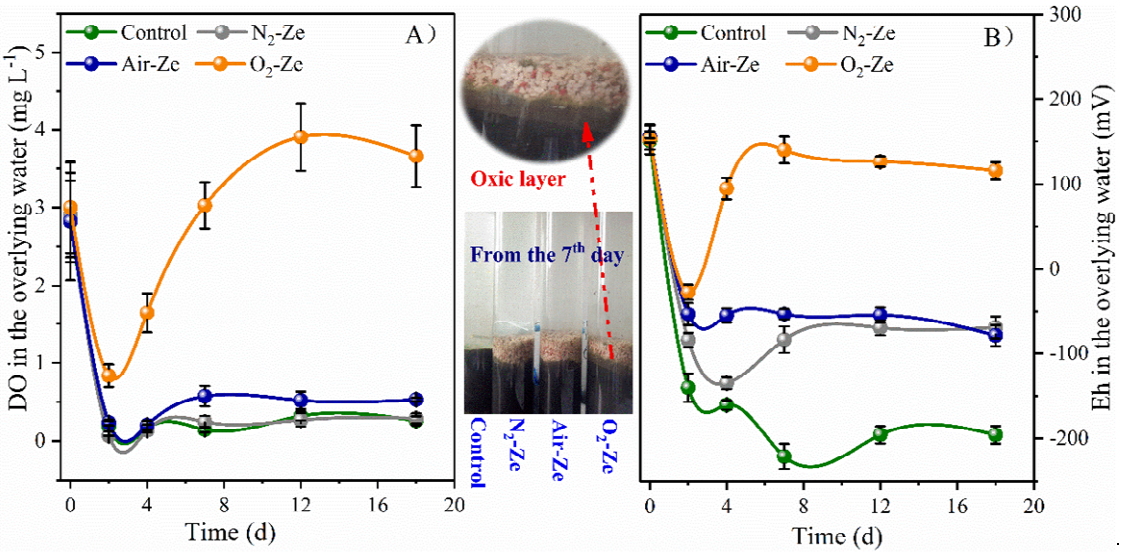

Fig. 1. Variation of DO (A) and Eh (B) in the overlying water during the experimental period

The simulated algal-induced hypoxia triggered an acute release of As from the sediment with total dissolved As levels reaching 23.2 μg L^{-1} in the overlying water by day 4 (Fig. 2A), exceeding twice the WHO's recommended As safety limit (10 μg L^{-1}) (Yan et al., 2016). The total dissolved As levels in the overlying water from the Air-Ze and N_2-Ze groups were lower than those in the control group, but still remained higher than 10 μg L^{-1} during the experiment (Fig. 2A), indicating that the physical capping by zeolites alone was not enough to control the endogenous release of As. Accompanying the hypoxic-oxic transition in the O_2-Ze group, the total dissolved As in the overlying water

remained at low levels, within the range of 6.97-9.72 μg L^{-1}. Moreover, the cumulative total dissolved As fluxes from sediment to water switched from positive (net As release) in the control (6.24 mg m^{-2}), N_2-Ze (2.88 mg m^{-2}) and Air-Ze (2.86 mg m^{-2}) groups to negative (net As retention) at -0.54 μg m^{-2} in the O_2-Ze group over the 18-day incubation period (Fig. 2B), demonstrating the successful change of sediment from As source to sink due to the synergistic effects of the formation of a physical barrier and the effects of O_2 nanobubbles originating from O_2-Ze. It should be noted that the oxidizing conditions at the SWI induced by O_2 nanobubbles also favoured As oxidation and methylation. The predominant As species changed from the more toxic form of As(III) in the control, N_2-Ze and Ze groups to lower toxicity forms of As(V) (65–75%) and methylated As (MMA(V) and DMA(V)) (10–15%) in the O_2-Ze group (Fig. 2A) thus further reducing the As exposure risk in the water column. Therefore, further investigation into possible mechanisms was focused on the comparison between control and O_2-Ze groups.

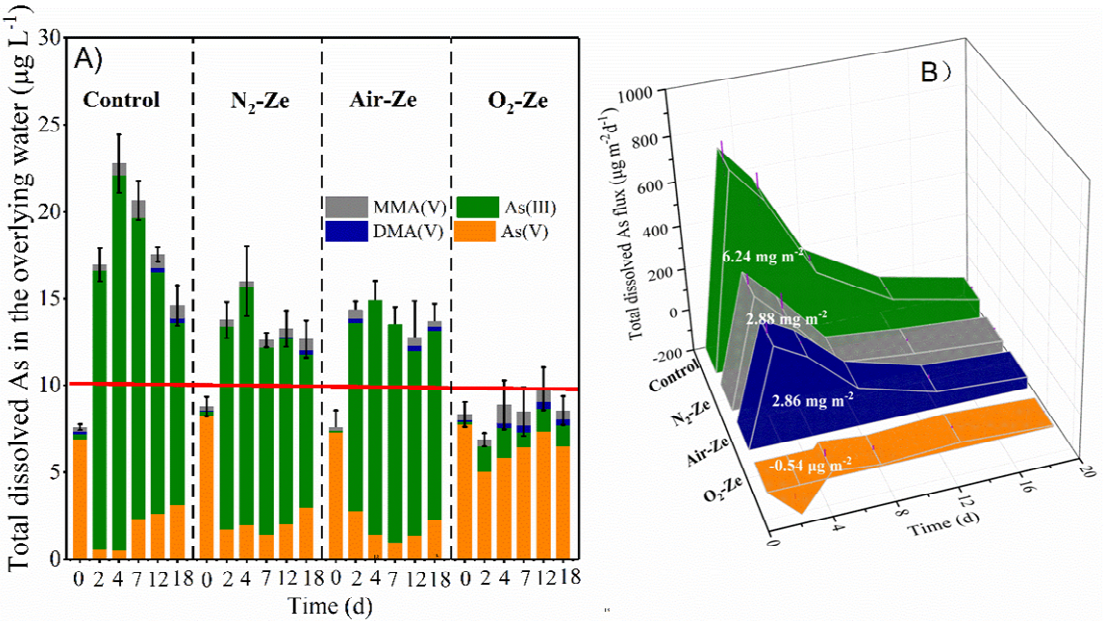

Fig. 2. As dynamics during the experimental period. (A) Total dissolved As in the overlying water. The red line indicates the WHO's recommended As safety limits of 10 μg L^{-1} in drinking water.

(B) Total dissolved As flux across the sediment-water interface. The data appears in a white font in each bar, indicating the cumulative total dissolved As flux during the 18-day incubation period.

3.2 As mitigation controlled by geochemistry

It has long been recognised that the geochemical cycle of As is strongly linked to complex interactions, with co-mobilisation of some other elements, such as iron and carbon, also present in the sediment (Zhu et al., 2017). In the control group, accompanying the endogenous release of total dissolved As (mainly As(III)) (Fig. 2A), the algal-induced hypoxia also triggered the release of large amounts of DOC (Fig. 3A) and total dissolved Fe (mainly Fe(II)) (Fig. 3B) from sediments to the overlying water. The dynamics of DOC and total dissolved Fe in the overlying water (Fig. 3A and 3B) and sediment porewaters (Fig. S3) followed the same trend and were significantly correlated with concentration changes in total dissolved As in these waters ($P < 0.05$; Fig. 3C). This result indicated the occurrence of microbial reductive dissolution of As-bearing Fe oxides with subsequent As release (Zhou et al., 2016), as triggered by the intensified hypoxic conditions and the presence of an abundance of organic matter acting as an electron donor at the SWI (Postma et al., 2012; Tang et al., 2019). However, during treatment with O_2-Ze, a distinct decrease of DOC in the overlying water (Fig. 3A)-was observed during the experimental period, when compared to the control. This may attribute to the oxidation reactions between DOC and dissolved O_2 or the possibly generated reactive oxidizing species (ROSs), such as •OH (Liao et al., 2019a; Page et al., 2013) at the SWI. The decrease of reactive organic carbon (e.g. glucose) at the SWI could further have inhibited the activity and growth of iron-reducing bacteria (Stuckey et al., 2016). Thus, oxidation of Fe(II) occurred both in the overlying water (Fig. 3B) and in surficial sediments (Fig.

S4B) compared to the control, and the regenerated Fe(III)-(hydr)oxides may have been responsible for As sequestration at the oxic SWI (Tong et al., 2016; Stuckey et al., 2016), leading to the combination of reduction in total dissolved As levels in overlying water and the inhibition of As release from surface sediments. This speculation was not only supported by the highly significant correlation between total dissolved Fe and As concentrations in water profiles (r = 0.631, P < 0.01; Fig. 3C), but also by a strong correlation between the spatial distribution of As and that of Fe in surface sediments in O_2-Ze group, observed through SR-μXRF analysis (Fig. 3D).

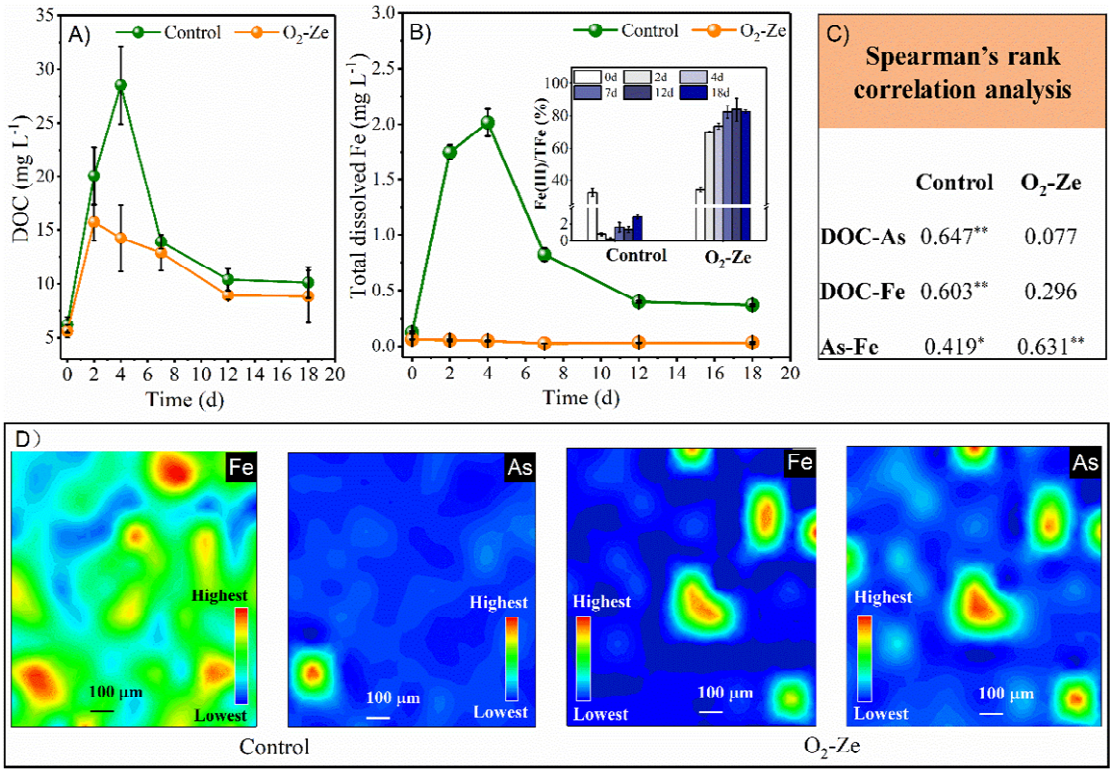

Fig. 3. Dynamic Geochemistry of As. (A) DOC (Dissolved Organic Carbon) in the overlying water; (B) Total dissolved Fe in the overlying water. The inset indicates the proportion of dissolved Fe (III) in the total dissolved Fe. (C) Spearman's rank correlation between total dissolved As, total dissolved Fe and DOC concentrations during the experimental period. Data for each correlation (n=24) consisted of concentrations taken from the overlying water and pore water profiles. Values of $P < 0.05$ and < 0.01 indicate significant (*) and highly significant (**) correlations, respectively. (D) As and Fe distributions in surficial sediments, observed by SR-

μXRF analysis.

In order to further quantify the variation of interaction between As and Fe in surficial sediments after O_2-Ze treatment, As and Fe K-edge XANES spectral analyses were conducted. Panels A and C of Fig. 4 illustrate the linear combination fitting (LCF) of Fe and As K-edge XANES spectra of surface sediments sampled after completion of the simulation experiment, and Fig. 4B and 4D summarize the LCF results, respectively. The results indicated that the oxic layer, generated on the surfacial sediments after O_2-Ze treatment, induced the rapid formation of ferrihydrite, the proportion of which increased from 6.9% to 38.1% (Fig. 4B). Ferrihydrite is one of the amorphous Fe(III)-oxyhydroxides that is ubiquitous in natural waters, especially at the redox boundaries of the SWI (Hoffmann et al., 2014). It is known to be an effective As absorbent, due to characteristics of nanometer-sized particles and high surface area (Tong et al., 2016; Stuckey et al., 2016). In this investigation, accompanied by the distinct oxidation of As(III) to As(V) in oxic surface sediments induced by O_2 nanobubbles (Fig. 4C and S4B), a significant increase (from 8.1% to 28.3%) in the generated As(V) adsorbed to ferrihydrite, compared with the control (Fig. 4D), was also observed. These results strongly confirmed that Fe-controlled sequestration was the primary inhibition mechanism of endogenous As release from As-bearing sediments under O_2-Ze treatment.

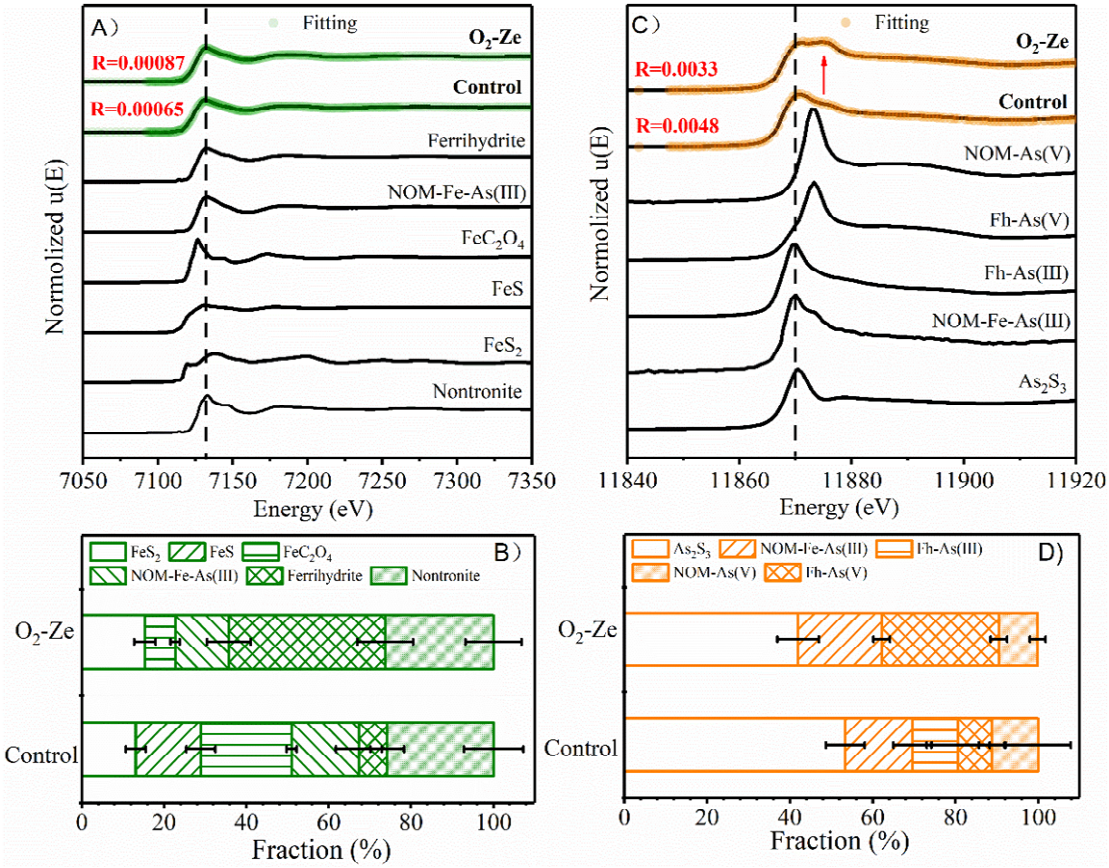

Fig. 4. As and Fe speciation in surface sediments. (A) and (C), Fe and As K-edge XANES spectra of the raw samples and reference compounds used for linear combination fitting (LCF) analyses, respectively. Experimental data are shown as solid black lines, and symbols represent LCF of the XANES spectra. R values show the mean square misfit between the data and the fit. (B) and (D), speciation of Fe and As in surface sediments, respectively. Speciation was obtained by LCF of K-edge XANES data and the component sums were normalized to 100%. Fh-As(III)/As(V) indicates ferrihydrite adsorbed As(III) or As(V).

3.3 Biotic- and abiotic-mediated As speciation

3.3.1 Biotic methylation of As

In unsterilized systems, the As methylation ratios along the whole experimental period achieved to 2.1-7.1% and 5.5%-14.7%-in the overlying water of control and O_2-Ze treatment-group, respectively (Fig. 5A). However, similar As methylation ratios (1.9-3.5%) were found in the overlying water in the two sterilized systems, i.e. S-O_2-Ze and

S-control groups. In particular, the As methylation ratios were significantly higher in the unsterilized systems compare with the corresponding sterilized systems from day 7 (Fig. 5A). These results supported the premise that methylation of As(III) to MMA(V) and DMA(V) after capping with O_2-Ze was a microbially-mediated process (Maguffin et al., 2015). Known as an effective method of As detoxification, As methylation has been demonstrated to be catalysed by a family of As(III) S-adenosylmethionine methyltransferase enzymes encoded by the *ars*M gene (Zhu et al., 2017). There are more than 30,000 entries for *ars*M sequences in the NCBI database in members of all kingdoms, including both aerobic and anaerobic microbes (Zhang et al., 2013; Zhu et al., 2014). In our investigation, abundances of the *ars*M gene in the water column increased significantly from 4.51×10^6 to 5.46×10^6 copies L^{-1} after the O_2-Ze treatment (Fig. 5B)~~,~~ ~~demonstrating~~. It may attribute to the enhanced growth of As(III) methylated aerobic microbes~~,~~ under the oxic condition at SWI induced by capping with O_2-Ze. Those methylated microbes can further ~~which may have been~~ responsible for the methylation of As(III) to DMA(V) and MMA(V) in the overlying water (Fig. 2A).

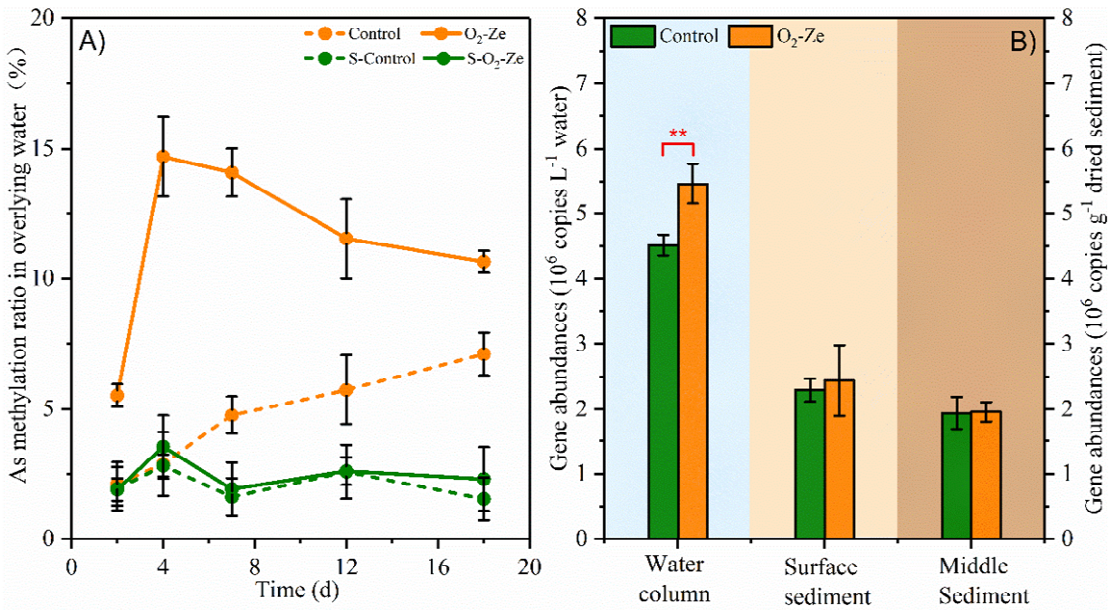

Fig. 5. Methylation of As at the SWI. (A) As methylation ratio in the overlying water in the sterilized and unsterilized systems. Methylation ratio of As was calculated by the concentration ratio of methylated As (i.e. DMA and MMA) and total dissolved As in the overlying water. (B) Gene abundances of *ars*M at the SWI. The symbol "**" represents $p < 0.01$ (independent t-test).

3.3.2 Biotic oxidation of As

Significantly higher As oxidation ratios in both overlying water and surface sediments were observed after hypoxia remediation by O_2 nanbubbles compared to the control in unsterilized systems (Fig. 6A and 6B). More importantly, the As oxidation ratio in the sterilised system under treatment by O_2-Ze also showed much higher levels, compared with the sterilised control group (Fig. 6A and 6B). These results supported the hypothesis that As oxidation induced by O_2 nanobubbles technology can be categorised as both a biotic process, mediated by functional microbial activity, as well as direct abiotic chemical oxidation at the oxic SWI. Generally, As oxidation in the sterilised systems can be considered an abiotic process, but one which accounted for 26.9-51.4% of the total As oxidation in the unsterilized system, based on the mass balance calculation (Fig. 6A and 6B). The remaining contribution of 52.5-73.1% could then be attributed to a biotic processes. The biotic oxidation ~~through microbial metabolism~~ of As depends on the microbes capable of~~, involves~~ As(III) oxidation and As(V) reduction. As(III) oxidation is usually catalysed by As(III) oxidases encoded by *aio*A genes, and As(V) reduction involves respiratory pathway mediated by *arr*A genes and detoxification pathway mediated by *ars*C genes (Tang et al., 2019; Zhang et al., 2015). In comparison to the control groups, capping with O_2-Ze facilitated a highly significant increase in *aio*A gene abundances from 1.14×10^6 to 3.78×10^6 copies L^{-1} in the water column, and from 1.38

$\times 10^6$ to 1.96×10^6 copies g^{-1} in surface sediments (Fig. 6C). This result indicated that the oxic SWI, induced by the introduction of O_2 nanobubbles, favoured the growth of indigenous As(III) oxidizing microbes, contributing to the biotic oxidation pathway of As from As(III) to As(V) (Fig. 6A and 6B) (Zhu et al., 2014). Simultaneously, the corresponding abundances of *arr*A and *ars*C genes at the SWI decreased significantly, implying that the oxic SWI also inhibited the microbial As(V) respiratory and detoxification reduction pathways (Zhang et al., 2015).

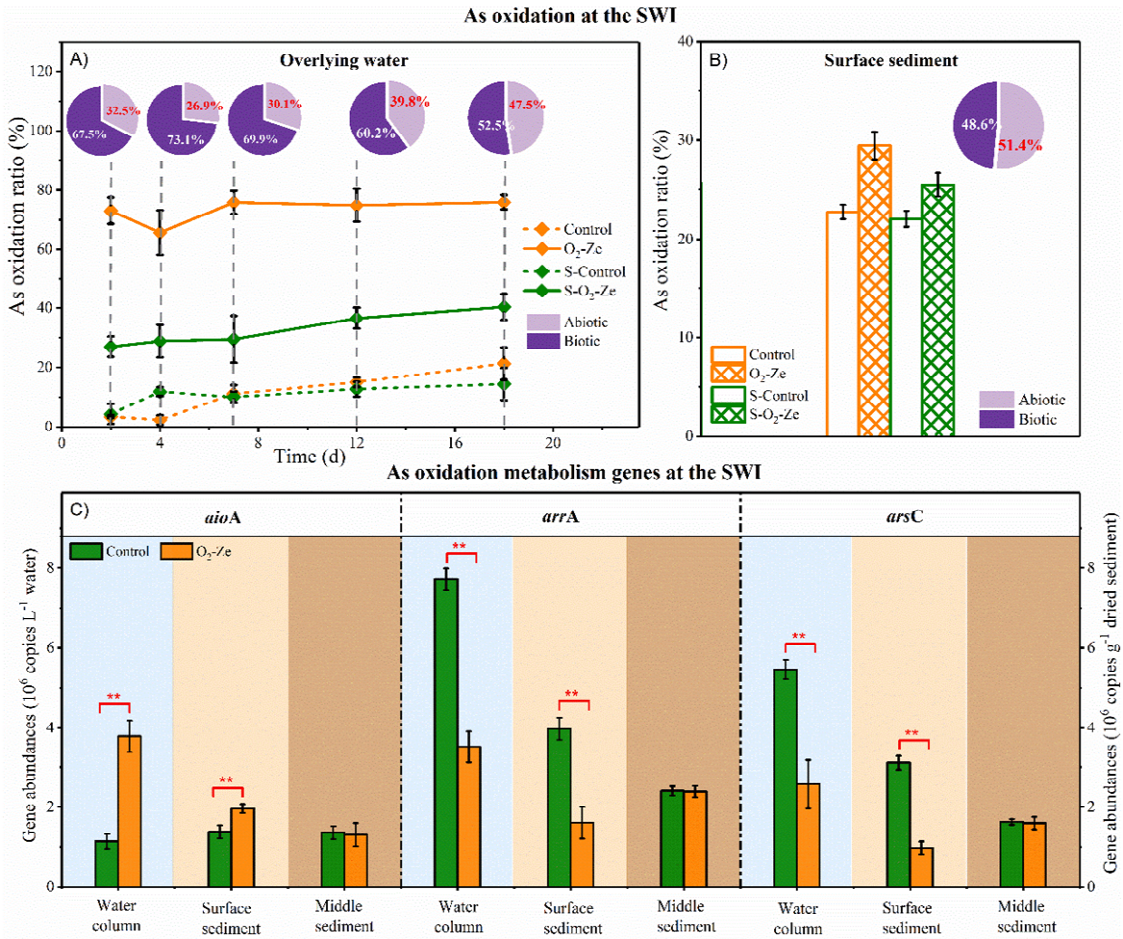

Fig. 6. Oxidation of As at the SWI. (A) As oxidation ratio in the overlying water for the sterilized and unsterilized systems. It was calculated by the concentration ratio of dissolved As(V) and total dissolved As in the overlying water. (B) As oxidation ratio in surface sediments for the sterilized and unsterilized systems. It was calculated by the concentration ratio of As(V) and TAs in the surface sediments. (C) Gene abundances of *aio*A, *arr*A and *ars*C at the SWI. The symbol"**"

represents $p < 0.01$ (independent t-test). The inset pie charts in (A) and (B) indicate the calculated contributions of abiotic and biotic As oxidation.

3.3.3 Abiotic oxidation of As

When O_2 nanobubbles were released from O_2-Ze at the hypoxic SWI, they may have influenced the abiotic oxidation of As(III) by directly forming •OH during natural bubble rupture (Atkinson et al., 2019), in addition to providing sufficient dissolved O_2 for sediment/water oxygenation at the SWI (Fig. 1A). Therefore, we initially attempted to measure the •OH forming capacity of pure water with O_2-Ze, but no distinct ESR •OH spectrum was detected (Figure S5). Given that the detection limit of ESR technique was usually 10^{-8} mol L^{-1} for paramagnetic species such as ROSs (Wang et al., 2011), this result indicated no, or extremely low, generation of •OH by natural bubble rupture from O_2-Ze, possibly due to the lack of •OH potentiating factors (e.g. UV irradiation or chemicals (such as H_2O_2)) in the waters (Liu et al., 2016). Therefore, it was considered that the dissolved O_2 supply was likely to be the dominant driver of abiotic oxidation of As(III) at the SWI.

Generally, abiotic oxidation of As(III) by dissolved O_2 is considered to be quite a slow reaction, with half-lives ranging from several months to a year (Smedley and Kinniburgh, 2002). However, this reaction can be catalysed in natural systems by the presence of redox-sensitive elements, such as Fe, Mn and C (Gorny et al., 2015). Recent studies have discovered the formation of •OH through Fenton or Fenton-like processes under dark conditions, once either Fe(II) or reduced organic matter in the anoxic water/sediments was exposed to, and oxidized by, dissolved O_2 (Tong et al., 2016). These reduced substances were abundant at the algal-induced hypoxic overlying water (Fig. 3A

and 3B) and surficial sediments (Fig. S~~3~~4 and Table S3), but subsequently underwent rapid oxidation after encountering dissolved O_2 originating from O_2 nanobubbles in the O_2-Ze group, suggesting the possibility of generation of •OH at the SWI. To further verify production of •OH during the oxidation of hypoxic water/sediment at the SWI and to qualitatively clarify its potential for As abiotic oxidation, an oxygenation experiment was conducted using a sterilized sediment-water slurry. The results indicated that when the hypoxic slurry was exposed to dissolved O_2, an ESR spectrum, containing four peaks with intensity ratios of 1:2:2:1, was observed, which could be compared to the ESR •OH spectrum produced by the traditional Fenton process (Fig. 7A), implying the generation of •OH.

Moreover, in the blank ~~control~~ group, the cumulative As oxidation ratio was approximately 14% within 48 h (Fig. 7B). After exposure to dissolved O_2, significantly higher cumulative As oxidation ratio~~s~~ of nearly 44% was achieved in the water. However, the oxidation ratio sharply decreased to 24% when ethanol, a •OH scavenger (Tong et al., 2016), was added during the oxygenation process (Fig. 7B). These results confirmed that •OH, generated from the oxidation of abundant reduced substances present in the sediment/water, rather than as a direct result of nanobubble rupture, would be the predominant contributor to abiotic oxidation of As in the O_2 nanobubble treatment. In addition to •OH, Fe(IV) may also play a role in the residual abiotic oxidation of As(III). Several studies have reported that Fe(IV) can be generated during interactions between Fe(II) and O_2 at neutral pH, leading to the co-oxidation of As(III) in interfaces at natural redox environments (Ding et al., 2018; Hug and Leupin, 2003). Thus, further research

should focus on the in-site monitoring of •OH and Fe(IV), in order to assessing their contributions to As speciation.

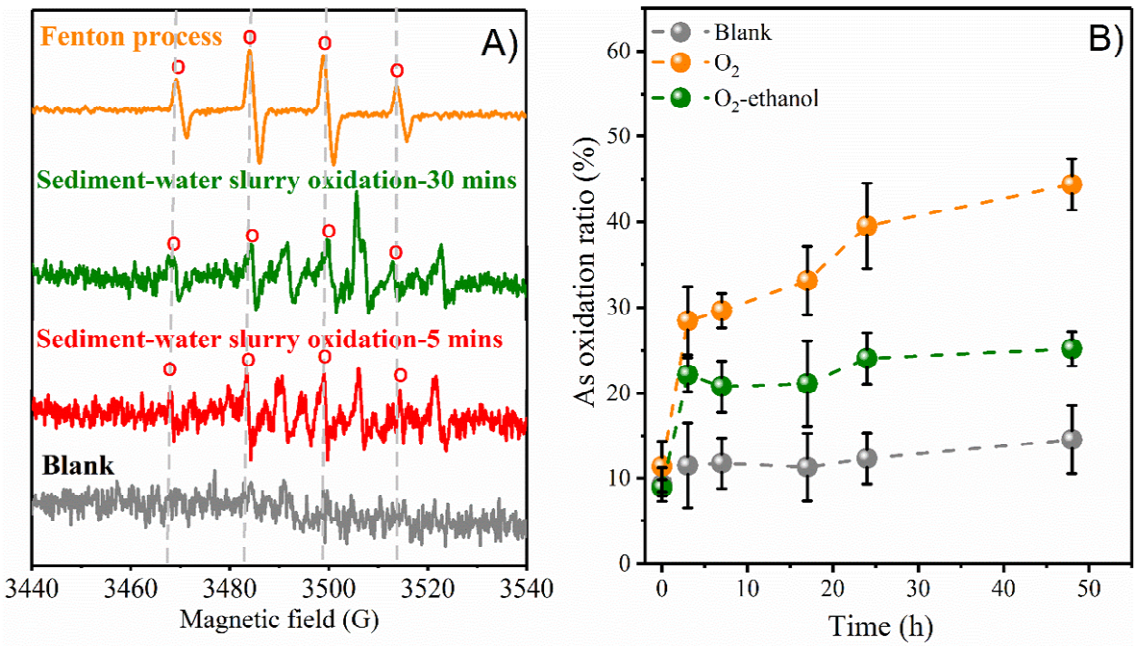

Fig. 7. Abiotic-mediated As speciation at the SWI. (A) ESR evidence of •OH production from oxygenation of sterilized sediment-water slurry. (B) As oxidation ratio in water during sterilized sediment-water slurry oxygenation (sediment/water=30 g/150 mL).

3.4 As fate under the treatment of O_2-Ze

In As-polluted eutrophic waters, where HABs problems are increasing (Hasegawa et al., 2009; Tang et al., 2019), anaerobic degradation of algae-induced organic matter at the SWI stimulates a contemporaneous release of As(III), Fe(II) and reduced organic matter into the water column (Fig. 2 and 3), leading to the risk of As pollution. Application of O_2 -Ze at the hypoxic SWI can induce rapid remediation of hypoxia. The resultant oxidizing conditions favored the growth of indigenous As(III) methylated (carrying the *ars*M gene) and oxidative (through the *aio*A gene) microbes at the SWI. The former microbes catalyzed the biotransformation of As(III) to MMA(V) and DMA(V), and the latter catalyzed the biotic oxidation of As(III) to As(V). The As(III) oxidation process was

also promoted by the reaction of As(III) with •OH, during which •OH can be produced by the oxidation of ferrous compounds and/or reduced organic matter in darkness. The resultant As(V), MMA(V) and DMA(V) have much lower toxicity than As(III) (Tang et al., 2019), which potentially reduce the risk of As exposure. Moreover, the rejuvenated ferrihydrite, at the oxidizing SWI, is highly efficient not only in stripping dissolved As(V) from the overlying water, but also in hampering the flux of As from sediments to the water column, thus further mitigating As pollution.

3.5 Environmental implications

Globally, HABs have been the cause of serious environmental disasters in hypereutrophic waters over recent years (Huisman et al., 2018). The resultant hypoxic/anoxic events have not only induced extensive mortality of benthos and fish, but have also caused elevated exposure of pollutants, including As (Tang et al., 2019). This study demonstrates that the proposed interfacial O_2 nanobubble technology has the capability to reverse the hypoxic conditions, by manipulating O_2-related microbial and geochemical processes to minimize the algal-induced As pollution risk in eutrophic waters. The hypoxia reversal effectiveness of this technology has proven to last for months in the earlier study (Zhang et al., 2018b), which may guarantee the long-term As mitigation effect. Although a cost of €0.5-1.5 million per km^2 was roughly calculated by using the interfacial O_2 nanobubble technology for sediment remediation in a previous study (Zhang et al., 2021), this estimation was also based on a lab-scale experiment. Therefore, optimised methodology for the material preparation and longer-term experiments in large-scale systems should be further investigated, in order to move

towards field application of the approach. This will enable a full cost-benefit analysis of the technology to be carried out.

Apart from the significant influence of O_2 nanobubbles on functional microbial activity of As, we also highlight the production of •OH in darkness, at the hypoxic SWI enriched with reductive substances and its dominant role in abiotic oxidation of As(III) during hypoxic-oxic transitions induced by dissolved O_2 from O_2 nanobubbles. This may provide insights for abiotic oxidative transformations of other redox-sensitive elements and chemical species (e.g. Hg, Cr, U, S , Fe, and antibiotics) in systems facing naturally- or artificially-hypoxic/anoxic-oxic transitions, for example, wetting and drying phenomena due to irrigation-evaporation cycles in wetlands (Gambrell, 1994) or tidal processes in estuaries and mudflats (Gonneea et al., 2014).

4. Conclusions

This study applied the use of interfacial O_2 nanobubble technology to combat the algal-induced hypoxia that achieves good performance for As mitigation in eutrophic waters. The hypoxic-oxic transition at SWI under O_2-Ze treatment manipulated microbes responsible for As oxidation and methylation, leading to a conversion of As(III) to As(V) and methylated As species with less toxicity. It can also stimulate the dark formation of •OH, which further dominantly contributed to abiotic oxidation of As(III). The generated As(V) was sequestrated by Fe-(hydr)oxide under the oxic condition, making surface sediments changed from being sources to acting as sinks of As. Thus it suggested that the proposed technology could provide an eco-friendly and promising method for restoration of algal-induced As pollution in eutrophic waters.

Declaration of Competing Interest

The authors declare that they have no known competing financial interests or personal relationships that could have appeared to influence the work reported in this paper

Author contributions

G.P. and Y.T. conceived the experiments, which were carried out by Y.T., who also carried out data interpretation and drafted the manuscript. M.Y.Z. provided support for the synchrotron radiation measurements, genetic testing, and for manuscript preparation. T.L., J.Z. and M.C. contributed to the paper preparation, modification and language polishing.

Acknowledgements

This work was supported by the National Key R&D Program of China (2017YFA0207204, 2018YFD0800305), National Natural Science Foundation of China (42007339, 21377003), Fundamental Research Funds for the Central Universities (SWU119009), and Strategic Priority Research Program of the Chinese Academy of Sciences (XDA09030203). We thank Y. G. Zhu and G. X. Sun for help with microbiological data analysis. We thank M. Tong for help with the design of the hydroxyl radical quenching experiments. We thank BSRF for providing the synchrotron beam time and L.R. Zheng and P.F. An for help in the collection of XANES data.

References

Atkinson, A.J., Apul, O.G., Schneider, O., Garcia-Segura, S., Westerhoff, P., 2019. Nanobubble technologies offer opportunities to improve water treatment. Accounts Chem. Res. 52(5), 1196-1205.

Bierlein, K.A., Rezvani, M., Socolofsky, S.A., Bryant, L.D., Wüest, A., Little, J.C., 2017.

Increased sediment oxygen flux in lakes and reservoirs: The impact of hypolimnetic oxygenation. Water Resour. Res. 53(6), 4876-4890.

Bormans, M., Marsalek, B., Jancula, D., 2016. Controlling internal phosphorus loading in lakes by physical methods to reduce cyanobacterial blooms: a review. Aquatic Ecology 50(3), 407-422.

Bormans, M., Maršálek, B. and Jančula, D. (2015) Controlling internal phosphorus loading in lakes by physical methods to reduce cyanobacterial blooms: a review. Aquat. Ecol. 50(3), 407-422.

Catalán, N., Casas-Ruiz, J.P., von Schiller, D., Proia, L., Obrador, B., Zwirnmann, E., Marcé, R., 2017. Biodegradation kinetics of dissolved organic matter chromatographic fractions in an intermittent river. J. Geophys. Res-Biogeo. 122(1), 131-144.

Couture, R.M., Gobeil, C., Tessier, A., 2010. Arsenic, iron and sulfur co-diagenesis in lake sediments. Geochim. Cosmochim. Ac. 74(4), 1238-1255.

Ding, W., Xu, J., Chen, T., Liu, C., Li, J., Wu, F., 2018. Co-oxidation of As(III) and Fe(II) by oxygen through complexation between As(III) and Fe(II)/Fe(III) species. Water Res. 143, 599-607.

Funkey, C.P., Conley, D.J., Reuss, N.S., Humborg, C., Jilbert, T., Slomp, C.P., 2014. Hypoxia sustains cyanobacteria blooms in the Baltic Sea. Environ. Sci. Technol. 48(5), 2598-2602.

Gambrell, R.P., 1994. Trace and toxic metals in wetlands-a review. J. Environ. Qual. 23(5), 883-891.

Gonneea, M.E., Charette, M.A., Liu, Q., Herrera-Silveira, J.A., Morales-Ojeda, S.M., 2014. Trace element geochemistry of groundwater in a karst subterranean estuary (Yucatan Peninsula, Mexico). Geochim. Cosmochim. Ac. 132, 31-49.

Gorny, J., Billon, G., Lesven, L., Dumoulin, D., Made, B., Noiriel, C., 2015. Arsenic behavior in river sediments under redox gradient: A review. Sci. Total Environ. 505, 423-434.

Guillemette, F., McCallister, S.L., del Giorgio, P.A., 2013. Differentiating the degradation dynamics of algal and terrestrial carbon within complex natural dissolved organic

carbon in temperate lakes. J. Geophys. Res-Biogeo. 118(3), 963-973.

Hasegawa, H., Rahman, M.A., Matsuda, T., Kitahara, T., Maki, T., Ueda, K., 2009. Effect of eutrophication on the distribution of arsenic species in eutrophic and mesotrophic lakes. Sci.Total Environ. 407(4), 1418-1425.

Hoffmann, M., Mikutta, C., Kretzschmar, R., 2014. Arsenite binding to sulfhydryl groups in the absence and presence of ferrihydrite: a model study. Environ. Sci Technol. 48(7), 3822-3831.

Huang, J.H., 2016. Arsenic trophodynamics along the food chains/webs of different ecosystems: a review. Chem. Ecol. 32(9), 803-828.

Hug, S.J., Leupin, O., 2003. Iron-catalyzed oxidation of arsenic(III) by oxygen and by hydrogen peroxide: pH-dependent formation of oxidants in the Fenton reaction. Environ. Sci. Technol. 37(12), 2734-2742.

Huisman, J., Codd, G.A., Paerl, H.W., Ibelings, B.W., Verspagen, J.M.H., Visser, P.M., 2018. Cyanobacterial blooms. Nat. Rev. Microbiol. 16, 471-483.

Jin, X., Bi, L., Lyu, T., Chen, J., Zhang, H., Pan, G., 2019. Amphoteric starch-based bicomponent modified soil for mitigation of harmful algal blooms (HABs) with broad salinity tolerance: Flocculation, algal regrowth, and ecological safety. Water Res. 165.

Johnston, S.G., Keene, A.F., Burton, E.D., Bush, R.T., Sullivan, L.A., 2011. Iron and arsenic cycling in intertidal surface sediments during wetland remediation. Environ. Sci. Technol. 45(6), 2179-2185.

Kay, P., 2011. Arsenic pollution: a global synthesis. Area 43(1), 118-119.

Lei, P.N., Luis M., Liu, Y.R., Zhong, H., Pan, K., 2019. Mechanisms of algal biomass input enhanced microbial Hg methylation in lake sediments. Environ. Int. 126, 279-288.

Li, Y.M., Fan, Y., Li, X.D., Wu, D.Y., 2017. Evaluation of zeolite/hydrous aluminum oxide as a sediment capping agent to reduce nutrients level in a pond. Ecol. Eng. 101, 170-178.

Liao, P., Liang, Y., Shi, Z., 2019a. Impact of divalent cations on dark production of hydroxyl radicals from oxygenation of reduced humic acids at anoxic–oxic interfaces. ACS Earth Space Chem. 3(4), 484-494.

Liao, P., Yu, K., Lu, Y., Wang, P., Liang, Y, Shi, Z., 2019b. Extensive dark production of hydroxyl radicals from oxygenation of polluted river sediments. Chem. Eng. J. 368, 700-709.

Liu, S., Oshita, S., Kawabata, S., Makino, Y., Yoshimoto, T., 2016. Identification of ROS produced by nanobubbles and their positive and negative effects on vegetable seed germination. Langmuir 32(43), 11295-11302.

Luong, V.T., Canas Kurz, E.E., Hellriegel, U., Luu, T.L., Hoinkis, J., Bundschuh, J., 2018. Iron-based subsurface arsenic removal technologies by aeration: A review of the current state and future prospects. Water Res. 133, 110-122.

Lyu, T., Wu, S., Mortimer, R.J.G., Pan, G., 2019. Nanobubble technology in environmental engineering: revolutionization potential and challenges. Environ. Sci. Technol. 53(13), 7175-7176.

Maguffin, S.C., Kirk, M.F., Daigle, A.R., Hinkle, S.R., Jin, Q., 2015. Substantial contribution of biomethylation to aquifer arsenic cycling. Nat. Geosci. 8(4), 290-293.

Page, S.E., Kling, G.W., Sander, M., Harrold, K.H., Logan, J.R., McNeill, K., Cory, R.M., 2013. Dark formation of hydroxyl radical in arctic soil and surface waters. Environ. Sci. Technol. 47(22), 12860-12867.

Pan, G., Lyu, T., Mortimer, R., 2018. Comment: Closing phosphorus cycle from natural waters: re-capturing phosphorus through an integrated water-energy-food strategy. J. Environ. Sci. 65, 375-376.

Pan, G., Miao, X., Bi, L., Zhang, H., Wang, L., Wang, L., Wang, Z., Chen, J., Ali, J., Pan, M., Zhang, J., Yue, B., Lyu, T., 2019. Modified local soil (MLS) technology for harmful algal bloom control, sediment remediation, and ecological restoration. Water 11(6).

Postma, D., Larsen, F., Thai, N.T., Trang, P.T.K., Jakobsen, R., Nhan, P.Q., Long, T.V., Viet, P.H., Murray, A.S., 2012. Groundwater arsenic concentrations in Vietnam controlled by sediment age. Nat. Geosci. 5(9), 656-661.

Shi, W., Pan, G., Chen, Q., Song, L.-R., Zhu, L., Ji, X., 2018. Hypoxia remediation and methane emission manipulation using surface oxygen nanobubbles. Environ. Sci. Technol. 52(15), 8712-8717.

Smedley, P.L., Kinniburgh, D.G., 2002. A review of the source, behaviour and distribution of arsenic in natural waters. Appl. Geochem. 17(5), 517-568.

Stigebrandt, A., Gustafsson, B.G., 2007. Improvement of Baltic proper water quality using large-scale ecological engineering. AMBIO: A Journal of the Human Environment 36(2), 280-286.

Stuckey, J.W., Schaefer, M.V., Kocar, B.D., Benner, S.G., Fendorf, S., 2016. Arsenic release metabolically limited to permanently water-saturated soil in Mekong Delta. Nat. Geosci. 9(1), 70-76.

Tang, Y., Zhang, M., Sun, G., Pan, G., 2019. Impact of eutrophication on arsenic cycling in freshwaters. Water Res. 150, 191-199.

Tong, M., Yuan, S., Ma, S., Jin, M., Liu, D., Cheng, D., Liu, X., Gan, Y., Wang, Y., 2016. Production of abundant hydroxyl radicals from oxygenation of subsurface sediments. Environ. Sci. Technol. 50(1), 214-221.

Wang, Z., Ma, W., Chen, C., Ji, H., Zhao, J., 2011. Probing paramagnetic species in titania-based heterogeneous photocatalysis by electron spin resonance (ESR) spectroscopy—A mini review. Chem. Eng. J. 170(2), 353-362.

Weber, F.A., Hofacker, A.F., Voegelin, A., Kretzschmar, R., 2010. Temperature dependence and coupling of iron and arsenic reduction and release during flooding of a contaminated soil. Environ. Sci. Technol. 44(1), 116-122.

Wu, J., Boyle, E., Sunda, W., Wen, L.S., 2001. Soluble and colloidal iron in the oligotrophic north Atlantic and North Pacific. Science 293(5531), 847.

Yan, C., Che, F., Zeng, L., Wang, Z., Du, M., Wei, Q., Wang, Z., Wang, D., Zhen, Z., 2016. Spatial and seasonal changes of arsenic species in Lake Taihu in relation to eutrophication. Sci.Total Environ. 563–564, 496-505.

Yu, P., Wang, J., Chen, J., Guo, J., Yang, H., Chen, Q., 2019. Successful control of phosphorus release from sediments using oxygen nano-bubble-modified minerals. Sci.Total Environ. 663, 654-661.

Zhang, H., Huo, S., Yeager, K.M., Xi, B., Zhang, J., He, Z., Ma, C., Wu, F., 2018a. Accumulation of arsenic, mercury and heavy metals in lacustrine sediment in relation to eutrophication: Impacts of sources and climate change. Ecol. Indic. 93,

771-780.

Zhang, H., Lyu, T., Bi, L., Tempero, G., Hamilton, D.P., Pan, G., 2018b. Combating hypoxia/anoxia at sediment-water interfaces: A preliminary study of oxygen nanobubble modified clay materials. Sci. Total Environ. 637-638, 550-560.

Zhang, H., Lyu, T., Liu, L., Hu, Z., Chen, J., Su, B., Yu, J., Pan, G., 2021. Exploring a multifunctional geoengineering material for eutrophication remediation: Simultaneously control internal nutrient load and tackle hypoxia. Chem. Eng. J. 406, 127206.

Zhang, R,L., Sun, G.X., Zhu Y.G., 2013. Effects of microbial processes on the fate of arsenic in paddy soil. Chinese Sci. Bull. 58(2), 186-193.

Zhang, S.Y., Zhao, F.J., Sun, G.X., Su, J.Q., Yang, X.R., Li, H., Zhu, Y.G., 2015. Diversity and abundance of arsenic biotransformation genes in paddy soils from southern China. Environ. Sci. Technol. 49(7), 4138-4146.

Zhou, Q., Zhang, Y., Lin, D., Shan, K., Luo, Y., Zhao, L., Tan, Z., Song, L., 2016. The relationships of meteorological factors and nutrient levels with phytoplankton biomass in a shallow eutrophic lake dominated by cyanobacteria, Lake Dianchi from 1991 to 2013. Environ. Sci. Pollut. Res. 23(15), 15616-15626.

Zhu, Y.G., Xue, X.M., Kappler, A., Rosen, B. P., Meharg, A. A., 2017. Linking genes to microbial biogeochemical cycling: lessons from arsenic. Environ. Sci. Technol. 51(13), 7326-7339.

Zhu, Y.G., Yoshinga, M., Zhao, F.J., Rosen, B.P., 2014. Earth abides arsenic biotransformations. Annu. Rev. Earth Pl. Sci. 42(1), 443-467.

Supporting information

Reducing arsenic toxicity using the interfacial oxygen nanobubble technology in sediment remediation

Ying Tang[a,b], Meiyi Zhang[b], Jing Zhang[b], Tao Lyu[c], Mick Cooper[d], Gang Pan[b,d,*]

[a] *Chongqing Key Laboratory of Soil Multi-Scale Interfacial Process, Department of Soil Science, College of Resources and Environment, Southwest University, Chongqing 400715, P. R. China*

[b] *Research Center for Eco-Environmental Sciences, Chinese Academy of Sciences, Beijing 100085, P. R. China*

[c] *Cranfield Water Science Institute, Cranfield University, College Road, Cranfield, Bedfordshire, MK43 0AL, UK*

[d] *Integrated Water-Energy-Food Facility (iWEF), School of Animal, Rural, and Environmental Sciences, Nottingham Trent University, Nottinghamshire NG25 0QF, UK*

**Corresponding author: gang.pan@ntu.ac.uk (G. Pan)*

This SI contains 12 pages, which includes 4 figures and 3 tables.

Table of contents

1. Materials and methods 33
1.1 Preparation of O_2 and N_2 nanobubble modified zeolites 33
1.2 Water and sediment measurement 34
1.3 Bulk As and Fe k-edge X-ray absorption near-edge structure (XANES) analyses 36
1.4 Synchrotron radiation microscopic X-ray fluorescence (SR-μXRF) analysis ... 38
1.5 As metabolism functional gene analysis 38
1.6 Evaluation of total dissolved As flux from sediment to lake water 40
2. Results and discussion 40
3. References 43

1. Materials and methods

1.1 Preparation of O_2 and N_2 nanobubble modified zeolites

Granular natural zeolites (∅1–3 mm) with high porosity were purchased from Yongjia Natural Minerals Ltd., Heibei, China and used as the target minerals. The specific surface area and average micropore size of the selected zeolites were 38.1 m^2/g and 5.69 nm, as determined by the Brunauer-Emmett-Teller (BET) method using a Micromeritics ASAP-2020 instrument (Micromeritics Inc, USA) (Zhang et al., 2018). The preparation of O_2 nanobubble modified zeolites (O_2-Ze) was consistent with a previous study (Pan et al., 2016). The natural zeolite was initially washed with deionized water and dried for 10 h at 90 °C, and subsequently for 4 h at 350 °C. The dried zeolites were then placed into a pressure-resistant and airtight vessel which was then evacuated to a pressure of -0.08 ~ -0.1MPa for 2 h in order to remove air from the micropores. Thereafter, pure O_2 (99.99%), was admitted into the container and held at a pressure of 0.12 - 0.15 MPa for 4 h. The process was repeated three times to achieve O_2 supersaturation in the micropores of zeolites. The O_2-loading capacity of the O_2-Ze was determined to be 21.2 mg g^{-1} by the method proposed by Wang et al. (2018). The concentration of nanobubbles (majority with <200 nm in diameter) in the water reached around 10^7 particles mL^{-1} within one day, after addition of O_2-Ze (Zhang et al., 2018). For comparison, N_2 nanobubble-modified zeolites were prepared by the same procedure but with replacement of O_2 by N_2 gas.

1.2 Water and sediment measurement

The field sampling details in Dianchi Lake are shown in Fig. S1A, and the characteristics of the original sediments and water were described in our previous study (Tang et al., 2019). Schematics of the lab-scale mesocosm cylinder experiment are illustrated in Fig. S1B, and the experimental conditions of the different treatment groups are summarised in Table S1 as follows.

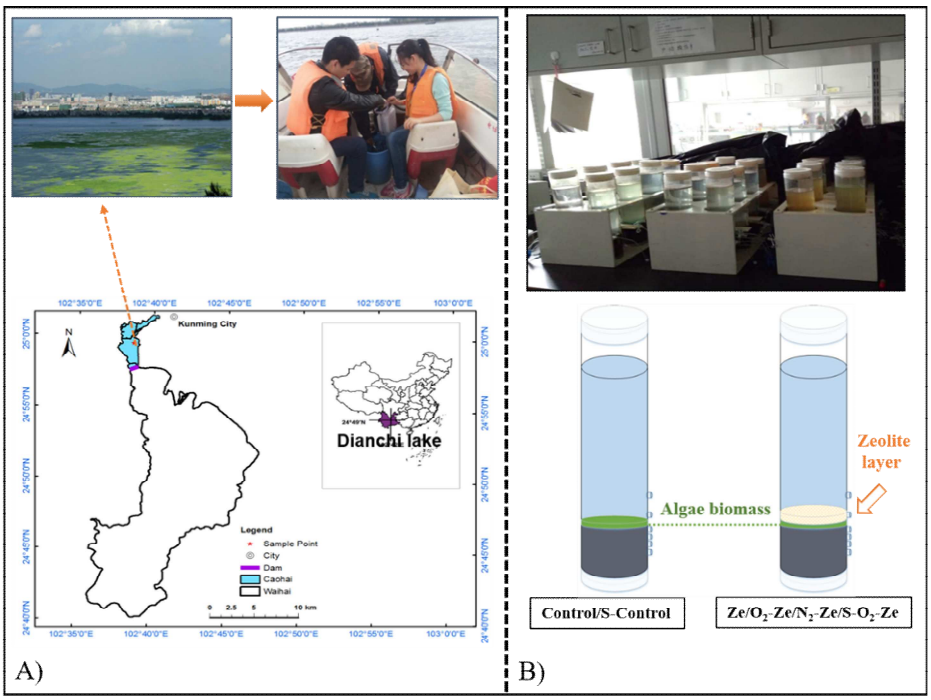

Fig. S1. Field sampling details in Dianchi Lake (A) and schematics of the lab-scale mesocosm cylinder experiment

Table S1 Experimental conditions of different treatment groups

No.	Group	Experiment condition
i	Control	Lake water-algae-sediment system
ii	Air-Ze	Lake water-algae-sediment system, capped with 2 cm (approximate 50 g) of pristine zeolites on the sediment surface
iii	N_2-Ze	Lake water-algae-sediment system, capped with 2 cm (approximate 50 g) of nitrogen nanobubble-modified zeolites on the sediment surface
iv	O_2-Ze	Lake water-algae-sediment system, capped with 2 cm (approximate 50 g) of oxygen nanobubble-modified zeolites on the sediment surface

v	S-control	Sterilized lake water-algae-sediment system
vi	S-O_2-Ze	Sterilized lake water-algae-sediment system, capped with 2 cm (approximate 50 g) of sterilized oxygen nanobubble-modified zeolites on the sediment surface

During the incubation period, DO (dissolved oxygen) levels at the sediment-water interface (SWI) was measured by dissolved oxygen analyzer (JPSJ-605, INESA Instrument Co. Ltd, China) and Eh (redox potential) by portable ORP meter (HI8424, Hanna Instruments, Italy). Samples of overlying water and porewater were analyzed for DOC (Dissolved Organic Carbon), dissolved Fe and As species. The DOC was measured by a TOC analyzer (enviroTOC, Elementar, Germany). The water samples for As analyses were acidified with HNO_3 after sampling, then analyzed using high-performance liquid chromatography attached to an Inductively-Coupled Plasma Mass Spectrometer (HPLC-ICP-MS) (iCAP Q, Thermo Scientific, USA). The dissolved Fe(II) and total dissolved Fe in the water samples were measured immediately after sampling, under dark conditions. The spectrophotometric methods employed have been commonly used for the analysis of iron content (Zhu et al., 2018). Due to the high sensitivity, the 1,10-phenanthroline method is used to measure the Fe(II) content at 510 nm using a UV-756 PC spectrophotometer (Shanghai Sunny Hengping Scientific Instrument Co. Ltd., China), and the total dissolved Fe concentrations were measured after first reducing Fe(III) to Fe(II) by hydroxylamine-HCl (Tong et al., 2016).

Total Fe(II) and total Fe in sediments were digested with 1.3 mol L^{-1} HF and 0.9 mol L^{-1} H_2SO_4 at 100 °C for 30 min in the dark (Neumann et al., 2008; Tong et al., 2016), and the extracted Fe analyzed, based on the aforementioned method for water samples. For the analyses of As(III) and total As concentrations in sediments, these

species were extracted by 1.2 mol L^{-1} HCl at 80 °C for 2 h (Tong et al., 2016), and the extracted As was determined by hydride generation atomic fluorescence spectrophotometry (AFS-9800, Jitian Instruments, China). Organic matter concentrations in sediment samples were determined by element analyzer (Vario EL cube, Elementar, Germany) after pretreatment with 1 mol L^{-1} HCl.

The production of •OH, either during natural bubble rupture in degassed ultrapure water during the O_2-Ze experiment or during the hypoxic sediment slurry oxygenation experiment was quantified by electron spin resonance (ESR), for which the water sample filtrate (passed through 0.45 μm membrane) of 950 μL was immediately mixed with 5,5-Dimethyl-1-pyrroline N-oxide (DMPO, 50 μL, 1.47 mol L^{-1}) to form the DMPO-OH adduct, and measured on a Bruker A300 EPR spectrometer (Bruker BioSpin GmbH, Germany) (Tong et al., 2016).

1.3 Bulk As and Fe k-edge X-ray absorption near-edge structure (XANES) analyses

Surficial sediments from the control and O_2-Ze groups were selected for bulk As and Fe K-edge XANES analyses. Fresh, homogenized sediment samples were placed into Plexiglas sample holders, sealed with Kapton® tapes and stored anaerobically until the measurements were complete. As K-edge (11.867 KeV) and Fe K-edge (7.112 KeV) XANES spectra were collected on beamline 1W1B at the Beijing Synchrotron Radiation Facility (BSRF, China). The instrument's Si (111) double-crystal monochromator was calibrated to the first-derivative maximum of the L3-edge adsorption spectrum of elemental Au (11.919 KeV) for As measurements, or to the K-

edge adsorption spectrum of elemental Fe (7.112 KeV) for Fe analysis. The appropriate metal foils were simultaneously measured along with the samples in order to account for any small energy offsets encountered during the measurements. The As spectra of the samples were collected in fluorescence mode using 19-element high purity solid-state Ge detectors (Canberra, Mirion Technologies, Georgia, USA), and the Fe spectra in transmission mode. For selected As and Fe reference compounds (Table S2), spectra were recorded in transmission mode. All spectra were energy calibrated, pre-edge subtracted, and post-edge normalized in Athena (Ravel and Newville, 2005), the percentages of the species in the samples were quantitatively determined by linear combination fitting (LCF) analyses. The reference spectrum used for LCF analysis was selected according to the general characteristics of the samples (Tang et al., 2019) and previous relevant researches (Hoffmann et al., 2013; Hoffmann et al., 2014; Langner et al., 2012; Xu et al., 2011). LCF analyses of Fe and As XANES spectra were performed over an energy range of -20 to +30 eV near the appropriate edge energy. Initial fit fractions were recalculated to yield a component sum of 100%.

Table S2 Reference compounds of As and Fe analyzed by XAS

Element	Compound	Chemical formula	Source/synthesis reference
Arsenic	Arsenic trisulphide	As_2S_3	CARS
	As(V)/As(III)-Ferrihydrite	—	Synthetic[#]
	As(V)-NOM	—	synthetic[#]
	As(III)-Fe-NOM	—	synthetic[#]
Iron	Fe(II)-oxalate dihydrate	$Fe(C_2O_4) \cdot 2H_2O$	commercial (Alfa Aesar)
	Fe monosulphide	FeS	commercial (Fluka)
	As(III)-Fe-NOM	—	synthetic[#]
	Ferrihydrite	FeOOH	synthetic[#]
	Pyrite	FeS_2	CARS
	Nontronite	—	*

CARS- Center for Advanced Radiation Sources, http://cars.uchicago.edu/xaslib/search

* The spectra of Nontronite was shared by Man Tong from State Key Laboratory of Biogeology and

Environmental Geology, China University of Geosciences.

[#] The synthetic methods have been previously described in our recent study (Tang et al., 2019).

1.4 Synchrotron radiation microscopic X-ray fluorescence (SR-μXRF) analysis

Fresh sediment samples were also used for SR-μXRF analyses. Preparation work was identical to that performed for the bulk As and Fe XAS analyses described earlier. SR-μXRF analysis of samples was conducted using beamline 4W1B at BSRF. The incident X-ray beam (15 keV) was generated using a Si (111) double-crystal monochromator, focused by a toroidal mirror and poly capillary lens to produce a spot size 50 μm in diameter. Mapping data of SR-μXRF were collected using a step size of 100 μm and with 10 s sampling per point. Total areas measured were 1000 μm × 1000 μm. SR-μXRF spectra were processed using the PyMCA software package (Solé et al., 2007). Elemental maps of the analyzed sections of the fresh sediments were processed using Origin 9.1 software (OriginLab Corp., USA).

1.5 As metabolism functional gene analysis

The abundance of the four As metabolism genes (i.e., *aio*A, *arr*A, *ars*C, and *ars*M) in overlying water column and sediment samples collected from 0-2 cm and 2-4 cm depth, were analyzed. Overlying water column samples were initially prepared by filtration through a 0.45 μm membrane (Whatman, UK), dissolution in PBS buffer solution (500 μL), and centrifugation (10 min, 1000 rpm). The supernatant (200 μL) was then used for DNA extraction. For sediment analyses, samples (1 g) were initially dissolved in PBS buffer solution (200 μL), centrifuged (10 min, 1000 rpm), and the supernatant DNA extracted using the mericon DNA Bacteria Kit and mericon DNA

Bacteria Plus Kit (Qiagen, Germany), according to the manufacturer's instructions. For each sample, three replicates were extracted separately. The DNA was dissolved in sterilized deionized water (30 μL) and stored at -20°C before use. The concentration of the extracted nucleic acids was measured by a NanoDrop 5000 UV-Vis spectrophotometer (Thermo Fisher Scientific, USA).

PCR amplification of those genes was performed with the primers described in our previous study (Tang et al., 2019). The three replicates of DNA extraction were PCR amplified in reaction mixtures (20 μL total volume; 2 μL 10x buffer, 0.8 μL dNTP mix, 1.6 μL primer F and R (0.8 μL of each), 2 μL DNA template, 0.2 μL Taq DNA Polymerase (5U/μL), 13.4 μL ddH_2O). PCR thermal cycling parameters for all genes were: 95°C (5 min) followed by 40 cycles (each 95°C, 10 s; 55°C, 45 s; 72°C, 1min). After cycling, reaction mixtures were further incubated (72°C, 10 min).

The abundances of the four genes from the targeted samples were estimated using the primers described earlier by quantitative real-time polymerase chain reaction (qPCR) performed using an ABI7500 Thermocycler (Applied Biosystems Inc., USA). The assays used the following reaction chemistry: 10 μL SYBR Green I mix, 0.4 μL ROX, 0.8 μL primer F+R (each 0.4 μL), 2 μL DNA template and 6.8 μL ddH_2O in a final volume of 20 μL. qPCR thermal cycling parameters were: 95°C (10 min) followed by 40 cycles (each 95°C, 10 s; 55°C, 1 min; hold 4°C). All quantitative PCR reactions were run in triplicate. Melting curve analyses were performed at the end of qPCR runs to check amplification specificity. Gene assay efficiencies were 127% for *aio*A-like, 116% for *arr*A, 114% for *ars*C and 125% for *ars*M. Standard curves ranging from 1×10^3 to

1×10^8 copies per reaction were generated from purified, linearized plasmids obtained from clone libraries.

1.6 Evaluation of total dissolved As flux from sediment to lake water

The average flux of total dissolved As across the SWI was calculated according to the following mass balance equation (Tang et al., 2019):

$$F_n = \frac{[V * (C_n - C_0) + \sum_i^n V_i * (C_i - C_a)]}{S * t}$$

Where F_n (μg m^{-2} d^{-1}) is the flux on the n^{th} sampling day, V (mL) is the volume of overlying water, C_n (μg L^{-1}) is the concentration of total dissolved As on the n^{th} sampling day, C_0 (μg L^{-1}) is the total dissolved As concentration before incubation experiment, V_i (mL) is the volume of sampling water, C_i (μg L^{-1}) is the total dissolved As concentration on the i^{th} sampling day, C_a (μg L^{-1}) is the total dissolved As concentration in the water added for maintaining the volume of water in the microcosm, S (m^2) is the cross sectional area of each microcosm and t(d) is the incubation time. The accumulated total dissolved As flux over the 18-day period was calculated by the trapezoidal method using MATLAB 9.4 software (Shi et al., 2018).

2. Results and discussion

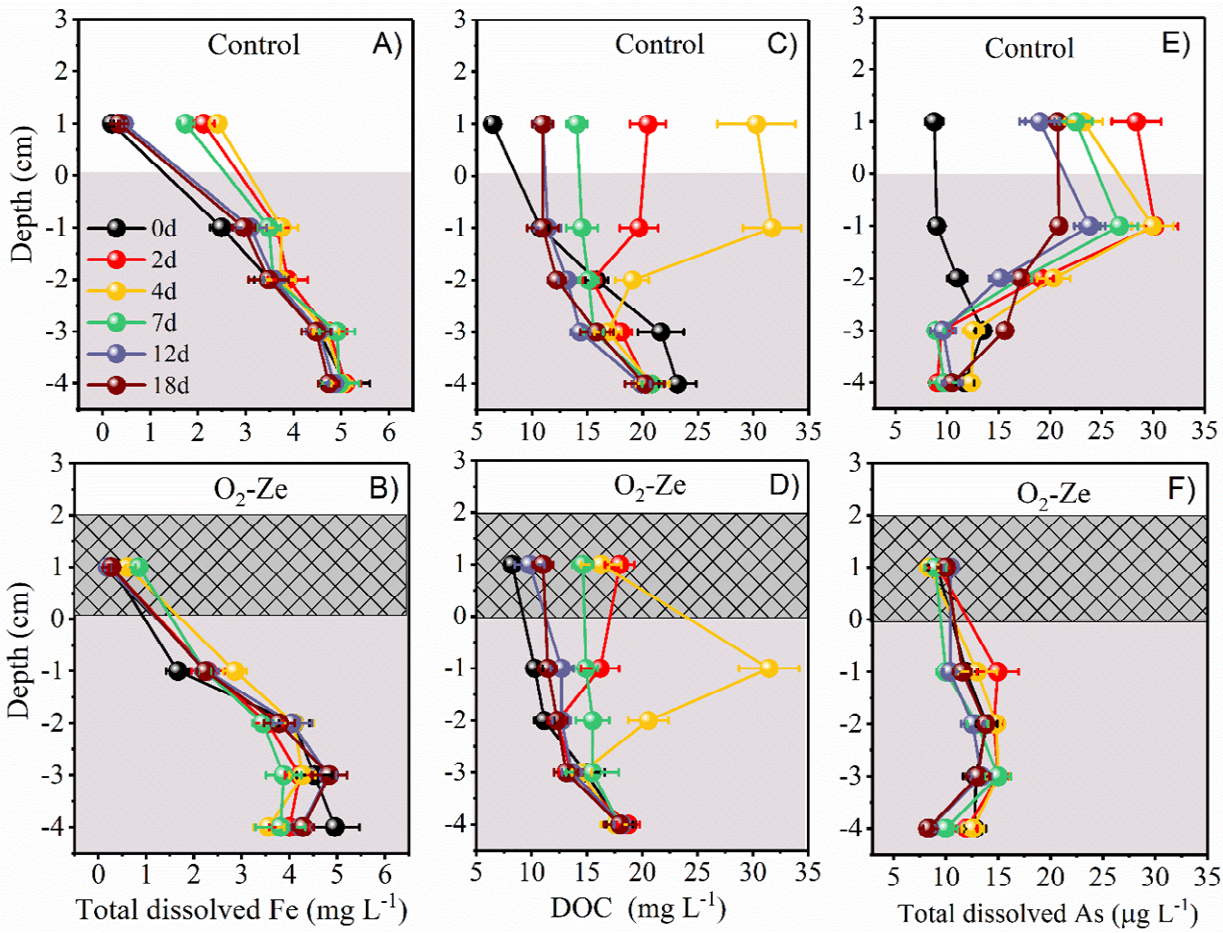

Fig. S2. Porewater profiles of total dissolved Fe (A-B), DOC (C-D), and total dissolved As (E-F) at the SWI during the experimental incubation period.

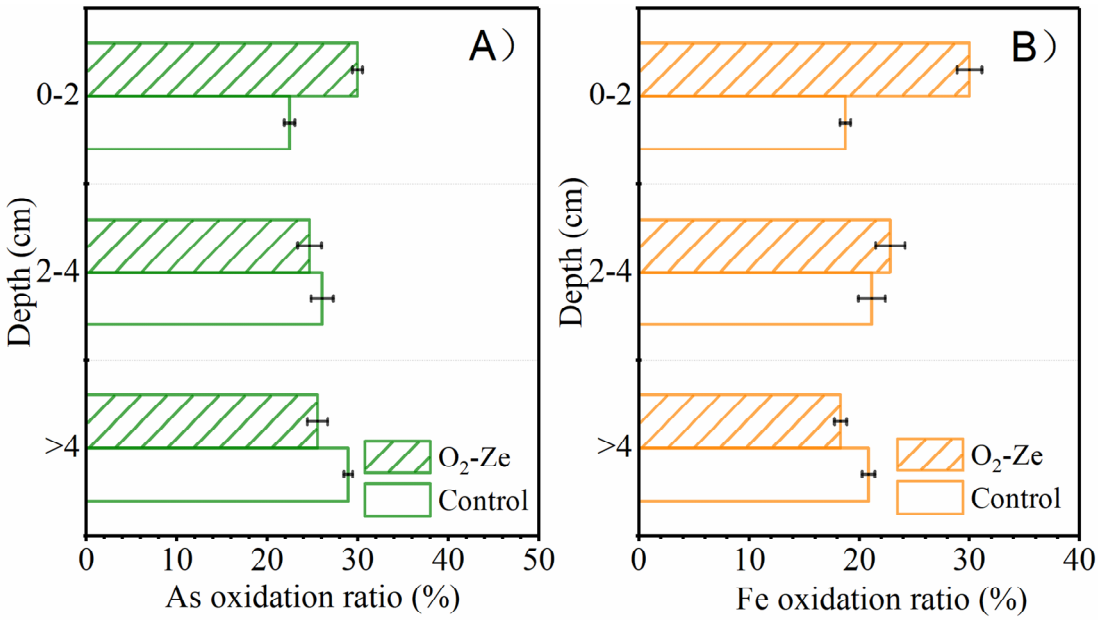

Fig. S3. As (A) and Fe (B) oxidation ratios in sediments at different depths

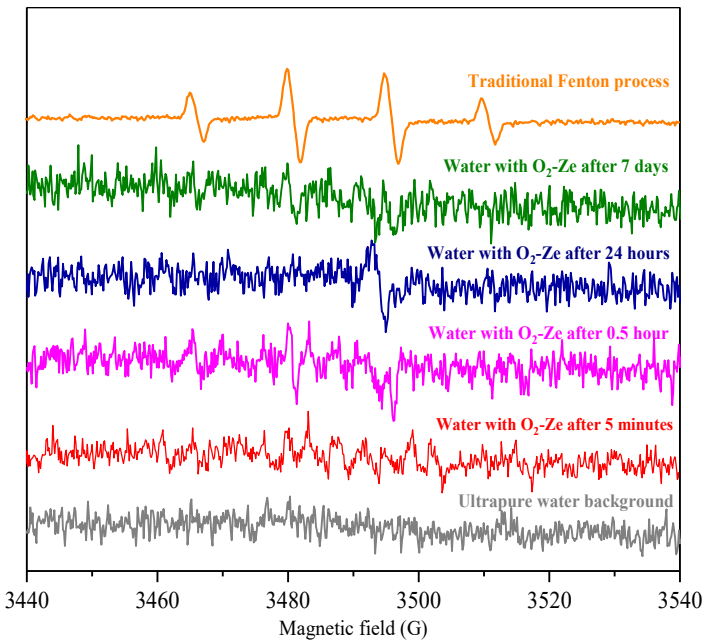

Fig. S4. ESR spectra of O_2-Ze in ultrapure water at different time points

Table S3 Total Organic Carbon (TOC) concentrations in sediments at different depths (%)

	Surface	Middle	Deep
Control	15.2±0.2	14.6±0.2	14.4±0.1
O_2-Ze	14.4±0.3	14.3±0.1	14.2±0.2

3. References

Hoffmann, M., Mikutta, C., Kretzschmar, R., 2013. Arsenite binding to natural organic matter: spectroscopic evidence for ligand exchange and ternary complex formation. Environ. Sci. Technol. 47(21), 12165-12173.

Hoffmann, M., Mikutta, C., Kretzschmar, R., 2014. Arsenite binding to sulfhydryl groups in the absence and presence of ferrihydrite: a model study. Environ. Sci. Technol. 48(7), 3822-3831.

Langner, P., Mikutta, C., Kretzschmar, R., 2012. Arsenic sequestration by organic sulphur in peat. Nat. Geosci. 5(1), 66-73.

Neumann, A., Hofstetter, T.B., Luessi, M., Cirpka, O.A., Petit, S., Schwarzenbach, R.P., 2008. Assessing the redox reactivity of structural iron in smectites using nitroaromatic compounds As kinetic probes. Environ. Sci. Technol. 42(22), 8381-8387.

Pan, G., He, G., Zhang, M., Zhou, Q., Tyliszczak, T., Tai, R., Guo, J., Bi, L., Wang, L., Zhang, H., 2016. Nanobubbles at hydrophilic particle-water interfaces. Langmuir 32(43), 11133-11137.

Ravel, B., Newville, M., 2005. ATHENA, ARTEMIS, HEPHAESTUS: data analysis for X-ray absorption spectroscopy using IFEFFIT. J. Synchrot. Radiat.12, 537-541.

Shi, W., Pan, G., Chen, Q., Song, L.R., Zhu, L., Ji, X., 2018. Hypoxia remediation and methane emission manipulation using surface oxygen nanobubbles. Environ. Sci. Technol. 52(15), 8712-8717.

Solé, V.A., Papillon, E., Cotte, M., Walter, P., Susini, J., 2007. A multiplatform code for the analysis of energy-dispersive X-ray fluorescence spectra. Spectrochimica Acta Part B: Atomic Spectroscopy 62(1), 63-68.

Tang, Y., Zhang, M., Sun, G., Pan, G., 2019. Impact of eutrophication on arsenic cycling in freshwaters. Water Res. 150, 191-199.

Tong, M., Yuan, S., Ma, S., Jin, M., Liu, D., Cheng, D., Liu, X., Gan, Y., Wang, Y., 2016. Production of abundant hydroxyl radicals from oxygenation of subsurface sediments. Environ. Sci. Technol. 50(1), 214-221.

Wang L., Miao.X.J., Jafar Ali, Lyu T., Pan G., 2018. Quantification of oxygen nanobubbles in particulate matters and potential applications in remediation of anaerobic environment. ACS Omega 3(9), 10624-10630.

Xu, L., Zhao, Z., Wang, S., Pan, R., Jia, Y., 2011. Transformation of arsenic in offshore sediment under the impact of anaerobic microbial activities. Water Res. 45(20), 6781-6788.

Zhang, H., Lyu, T., Bi, L., Tempero, G., Hamilton, D.P., Pan, G., 2018. Combating hypoxia/anoxia at sediment-water interfaces: A preliminary study of oxygen nanobubble modified clay materials. Sci. Total Environ. 637-638, 550-560.

Zhu, J., Yang, X., Fan, F., Li, Y., 2018. Factors affecting the determination of iron species in the presence of ferric iron. Applied Water Science 8(8).

https://dspace.org/

Reducing arsenic toxicity using the interfacial oxygen nanobubble technology for sediment remediation

Tang, Ying; Zhang, Meiyi; Zhang, Jing; Lyu, Tao; Cooper, Mick ...

2021-09-11
Elsevier
https://doi.org/10.1016/j.watres.2021.117657
Tang Y, Zhang M, Zhang J, et al., (2021) Reducing arsenic toxicity using the interfacial oxygen nanobubble technology for sediment remediation. Water Research, Volume 205, 15 October 2021, Article number 117657

Downloaded from a DSpace repository. https://dspace.org/